




Cite this: DOI: 10.1039/c7ta09028e

Received 13th October 2017
Accepted 16th December 2017

DOI: 10.1039/c7ta09028e

rsc.li/materials-a

Aligning the binder effect on sodium–air batteries†

Qian Sun, Xiaoting Lin, Hossein Yadegari, Wei Xiao, Yang Zhao, Keegan R. Adair, Ruying Li and Xueliang Sun *

Sodium–air batteries are attracting increasing research interest due to their high theoretical energy density and environmentally benign characteristics. Although sodium–air batteries share a similar concept, design, and composition when compared with their lithium–air counterparts, they still show many differences in their electrochemical behaviors and mechanisms. In the present work, the employment of four different types of polymers as binders in air electrodes for sodium–air batteries is presented, while the electrochemical and physical characterizations are carried out. Insights into how polymer binders impact the reaction mechanisms and formation of superoxide/peroxide species of sodium–air batteries from the view of their functional groups are revealed.

Introduction

The sodium–air battery (SAB) is a novel type of energy storage device belonging to the alkali metal–air battery family,^{1–8} which, along with the lithium–air battery (LAB)^{9–12} and potassium–air battery (PAB),^{13–15} is receiving ever-rising research attention due to its advantages over modern commercial power supplies such as high theoretical energy density and environmentally benign characteristics. Despite their similar concepts and cell constructions, the final oxidation states of oxygen in the discharge products of LABs, SABs, and PABs are reported to differ greatly. Li₂O₂ has been detected as the major discharge product of LABs,^{9–11,16} while KO₂ is primarily found in discharged PAB cells.^{13,14} However, several discharge products including NaO₂,^{17–24} Na₂O₂ or Na₂O₂·2H₂O,^{25–32} and/or Na₂CO₃ (ref. 33 and 34) have been reported for SABs. The observations regarding the formation of different discharge products in Na–air/O₂ batteries is still under investigation and may be related to various factors, such as kinetic and thermodynamic relationships,³⁰ chemical reactions,^{21,35} decomposition of solvent in the presence of superoxide,^{36,37} donor numbers of the solvents,^{38,39} and the types of carbon air electrodes.^{40,41} Previously, Nazar and co-workers have shown that proton donors are critical toward the favourable formation of cubic NaO₂ discharge products through a solution-mediated route,⁴² as directly evidenced by electron spin resonance (ESR) spectroscopy,⁴³ while also supported by the studies of other groups.^{20,44} Meanwhile, recent studies show that the configuration of the cells⁴⁵ and the use of a catalyst^{46–50} can all play an important role in the electrochemical performance and/or final composition of the

discharge products of SABs. The formation of discharge products in a superoxide phase has been preferred in both LABs and SABs due to their corresponding low charge overpotentials. However, the instability of the components of these air batteries (*i.e.* electrolyte solvent,^{4,9,51} salt,^{52–54} carbon air electrodes,^{37,55} and binders^{56–59}) toward superoxide/peroxide species leads to various side reactions and results in limited cycle life. Among these components, the binder plays an important role in the composition of most powder-based air electrodes for LABs and SABs. Binders are generally composed of a polymer used to bond catalysts and supporting carbon substrates to ensure the structural integrity of the air electrodes for alkali metal–air batteries. Up until now, binders for air electrodes have been selected based on those widely used in Li-ion batteries, such as polyvinylidene fluoride (PVDF). Nevertheless, it was first noticed by Nazar and co-workers⁵⁶ that in the environment of LABs, the PVDF binder is unstable in the presence of superoxide species, and decomposes through the following route: LiO_{2(s)} + -(CH₂-CF₂)_(s) → HO₂ + -(CH=CF)_(s) + LiF_(s). Since then, more detailed studies on identifying the stabilities of a large number of different polymer binders have been carried out by Nasybulin *et al.*⁵⁷ and Amanchukwu *et al.*⁵⁸ Nasybulin *et al.* investigated eleven types of polymers from both chemical and electrochemical aspects.⁵⁷ They ball-milled the polymers with Li₂O₂ and KO₂, and examined the products by X-ray photoelectron spectroscopy (XPS) and X-ray diffraction (XRD). In addition, they tested the electrochemical performance of the air electrodes containing the corresponding polymer binders and Ketjenblack (KB) carbon black in LABs. Amanchukwu *et al.* focused on the reactivity of the polymer binders in *N,N*-dimethylformamide (DMF) solutions against Li₂O₂ by Fourier transform infrared spectroscopy (FT-IR) and ultraviolet-visible spectroscopy (UV-Vis) characterizations, as well as their dimethyl sulfoxide (DMSO) solutions for nuclear magnetic resonance (NMR) characterization.⁵⁸ Most of the common

Department of Mechanical and Materials Engineering, University of Western Ontario, London, Ontario, N6A 5B9, Canada. E-mail: Xsun@eng.uwo.ca

† Electronic supplementary information (ESI) available. See DOI: 10.1039/c7ta09028e

polymers used as binders, *e.g.* PVDF, polyethylene oxide (PEO), carboxymethyl cellulose (CMC), polyvinylpyrrolidone (PVP), polystyrene (PS), polyacrylonitrile (PAN), polyvinyl chloride (PVC) and poly(methyl methacrylate) (PMMA), are found to be unstable against superoxides and/or peroxides. Meanwhile, polyethylene (PE), Nafion, and polytetrafluoroethylene (PTFE) are found to be relatively stable. However, it was noted by Nasybulin *et al.*⁵⁷ that even though PE was found to be among the most stable polymers against superoxide/peroxide species, the Li-O₂ battery assembled with a PE binder did not exhibit a significant improvement in terms of cycle life compared to the cell assembled with a PVDF binder. This implies that the reactivity of the binder in a practical cell may be more complicated than what is suggested by its general chemical stability. Therefore, a fundamental understanding of the role of binders and their contributions to the reaction mechanisms in SABs is still highly desired. Actually, it is worthy to note that Reeve *et al.* have very recently reported that grounding of NaO₂ with electrodes containing PVDF resulted in the decomposition of PVDF evidenced by the formation of NaF as revealed based on solid-state ²³Na NMR spectroscopy.⁶⁰ Nonetheless, to the best of our knowledge, a systematic experimental investigation on the effect of binders in practical SABs is still lacking up to now.

In the present work, we will report the usage of four different types of polymers, *i.e.* PE, PVP, PEO, and PMMA, as binders for air electrodes. The electrochemical behaviour of these air electrodes is examined in SABs. The influence of the polymer binders on the morphologies of discharge products is also revealed. We will aim at aligning the electrochemical response of air electrodes with different binders towards their known stabilities/reactivities as well as interpreting the role of functional groups on the polymer backbones.

Experimental

Preparation of air electrodes

Herein we use carbon nanotubes (CNTs) as the model material, same as our previous study on the effects of humidity on SABs,⁶¹ due to CNTs being one of the most commonly used air electrode materials for SABs.^{21,32,62–66} Commercial CNT powders were washed with hot nitric acid to remove the residual metallic catalyst before use. Commercial polymers were purchased from Sigma-Aldrich. PE, PMMA, PVP, and PEO were dissolved in toluene, acetonitrile, methanol, and acetonitrile solvents with a concentration of 50 mg mL⁻¹, respectively. Afterwards, CNT powders were mixed with the different polymer solutions in the CNT : binder weight ratio of 8 : 2 and ground before casting on commercial separator film substrates (Celgard 3501). The air electrodes were cut into round pieces with a diameter of 3/8 inch. The total mass loading of CNTs and binders in the air electrodes were in the range between 0.10 and 0.30 mg. The weight precision is ±0.01 mg.

Assembly of Na-air cells

Swagelok-type design of Na-air cells was adopted in this study as described in our previous work.⁶¹ A typical cell was composed

of a metallic sodium foil anode, polypropylene separator (Celgard 3501), and CNT air electrode with different binders. The electrolyte was 0.5 M sodium triflate (NaSO₃CF₃, Sigma-Aldrich) dissolved in diethylene glycol dimethyl ether (DEGDME, Aldrich). DEGDME was dried over molecular sieves (4 Å, Aldrich) for at least one month before use.

Electrochemical and physical characterization

The discharge/charge cycling measurements of SABs were performed using an Arbin BT-2000 battery station. The air cells were stored in a sealed box filled with 1.0 atm dry air at room temperature for cycling.⁶¹ Cyclic voltammetry (CV) measurements were carried out with a CHI 600 (CH Instruments, Inc). The morphologies of the discharge products were observed by using a Hitachi S-4800 field-emission scanning electron microscope (SEM). X-ray diffraction (XRD) measurements were carried out using a Bruker D8 Advance (Cu-K α source, 40 kV, 40 mA) spectrometer. Fourier transform infrared (FT-IR) spectra were measured using a Nicolet 380 (Thermo Scientific).

Results and discussion

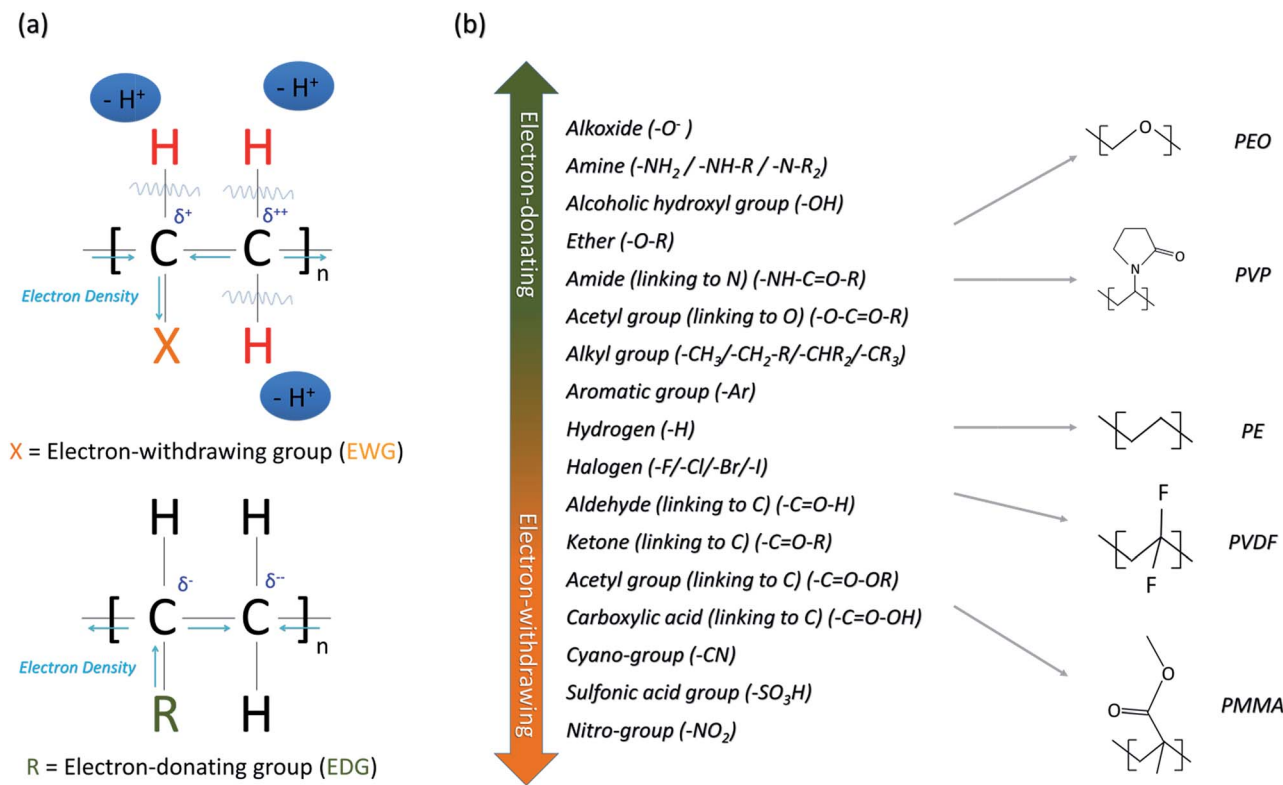
Fundamental hypothesis

It is well acknowledged that the properties and chemical reactivity of polymers are highly dependent on the functional groups in their main/side chains.^{67–69} In this study, we will aim at interpreting the role of polymer binders in SABs from a viewpoint of organic chemistry, *i.e.* the electron-withdrawing or electron-donating attributes of the corresponding functional groups, in a similar way as Amanchukwu *et al.*⁵⁸

In Lewis acid–base theory, a Lewis acid (acceptor) is defined as any substance that has the ability to accept non-bonding electrons, while a Lewis base (donator) is defined as any substance that has the ability to donate lone-pair electrons. In organic chemistry, Lewis acids and bases are generally used as electrophiles and nucleophiles, respectively, which builds the fundamental understanding on mechanisms of organic reactions. In brief, many organic reactions can be classified as the reactions between electrophile(s) and nucleophile(s).⁷⁰

Electron-withdrawing groups (EWGs) and electron-donating groups (EDGs) are the functional groups that either “pull” or “push” the electron density from or to the neighbouring atoms, respectively, as a result of resonance and inductive effects. The introduction of EWGs and EDGs can not only change the reactivity (nucleophilicity/electrophilicity) of the adjacent carbon (α -C) to which the functional group directly links, but also the other neighbouring atoms (*e.g.* α -H and β -C) linked to the α -C site (Scheme 1(a)). The electron donating/withdrawing capabilities of common functional groups are shown in Scheme 1(b).

On the other hand, according to molecular orbital (MO) theory, the structure of molecular oxygen O₂, the superoxide ion O₂⁻, and the peroxide ion O₂²⁻ can be described as shown in Scheme 2, with 2, 3, or 4 electrons filled in their two anti-bonding orbitals π^* , respectively. It is known that the filling of antibonding orbitals results in decreased bond order and



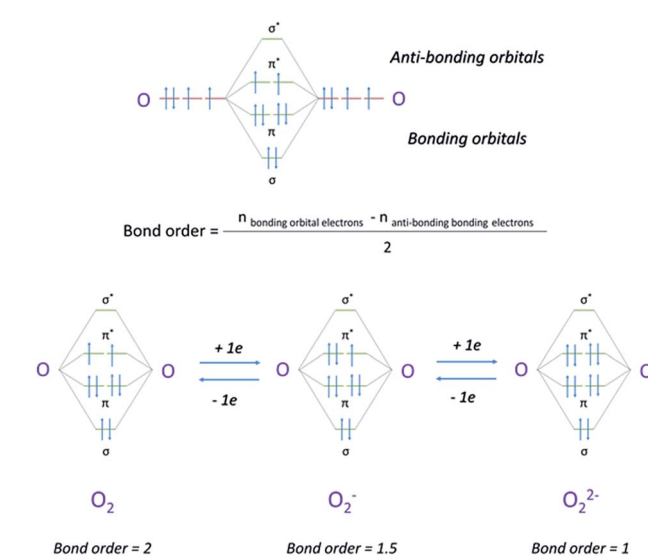
Scheme 1 (a) Schematic of the electron density redistribution of the polymer with an electron-withdrawing group (EWG) or an electron-donating group (EDG); (b) ranking of the strength of the EDGs and EWGs.

therefore reduced stability of covalent bonding. However, due to the much lower bonding–antibonding orbital splitting energy of π -type orbitals compared to σ -type, peroxides and superoxides are still relatively stable. Nevertheless, further donation of an electron to the σ^* orbital of O_2^{2-} often results in breaking of the covalent bond between the two oxygen atoms. These properties can explain the reactivity of O_2 , O_2^- , and O_2^{2-} in organic chemistry: O_2 mainly acts as an electrophile; O_2^{2-} acts mostly as nucleophile; O_2^- can play the role of both to either accept or donate an electron.^{71,72} Actually, it is worth noting that in aprotic solvents O_2^- is found to be more stable than O_2^{2-} .⁷¹ Therefore, the tendency of O_2^- as an oxidizing agent is not strong unless the formed peroxide products are stabilized by proton H^+ or metal ions such as Li^+ or Na^+ .⁷¹ Instead, O_2^- is more likely to be involved in nucleophilic substitution and hydrogen elimination reactions to produce HO_2^-/HO_2 and radicals or carbanions.⁷²

The nucleophilicity of O_2^- , and O_2^{2-} formed in LABs and SABs results in the chemical attack of solvent molecules. This has led to the switch from carbonate-based to ether-based electrolytes in the studies of these fields.^{73–75} Although ethers are not yet believed to be completely stable against peroxide/superoxide species,^{76–78} their side reactions are found to accumulate mostly during prolonged cycling.⁷⁹ Thus, ether electrolytes have become the most common choice for current studies on LABs/SABs,^{80,81} in spite of concerns of their negative effects on long-term cycling stability. Recently, Zhao and Guo revealed the relationship between the acid dissociation constants (pK_a) of solvents and the proportions of superoxide in the

corresponding discharge products of SABs.⁸² It is interesting to note that they found the existence of 92.68% NaO_2 in the SABs with TEGDME electrolyte, but this number sharply reduced to 8.92% for the one with an EC/PC electrolyte.

On the other hand, the existence of a trace amount of $H^+/H_2O/HO_2$ is found to be beneficial or even essential for LABs and SABs. It is reported that the introduction of water can



Scheme 2 MO diagram of O_2 , O_2^- , and O_2^{2-} .

significantly increase the discharge capacity of LABs, resulting in the formation of LiOH.^{83–85} When carefully controlled, the production of Li₂O₂ instead of side products can be promoted.^{86,87} Nazar and co-workers show that small traces of water (typically around 10 ppm) in ether electrolyte is the key for obtaining reasonable capacity as well as reversible decomposition of NaO₂ at low overpotentials. Actually, they show that the cell charging NaO₂ in an electrolyte with 0 ppm water exhibits a combination of two voltage plateaus around 2.7 V and 4.2 V, in contrast to the single charge voltage plateau around 2.5 V for the cell with 10 ppm water. Meanwhile, our group has also found that increased amounts of water from the gas source result in the formation of NaOH and Na₂CO₃, which prevents the reversible cycling of the cells.⁶¹ These results imply that the water in SABs is a double-edged sword, which needs to be optimized and carefully controlled.

Similarly, when moving on to explore the effect of O₂⁻ and O₂²⁻ on polymer binders, it should be taken into consideration that the reaction routes may also be expected to involve nucleophilic substitution and hydrogen elimination reactions,^{57,58} which can be enhanced by the introduction of EDGs/EWGs. As a result, H⁺, H₂O, HO₂, HO₂⁻, *etc.* may be released and impact the capacity, reversibility, oxygen reduction/evolution mechanisms, and composition of the discharge products of SABs with different binders. These reaction mechanisms and the effects of the EDGs/EWGs are the basis for the design of this study.

Selection of the polymers

Herein we pick four typical polymers (PE, PVP, PEO, and PMMA) for this study, which contain none or different types of electron donating/withdrawing functional groups that have been known to exhibit different chemical stabilities against Li₂O₂ and KO₂. Among them, PE is believed to be one of the most stable binders against peroxides and superoxides;⁵⁷ PVP is unstable towards both,^{57,58} PEO and PMMA are found to be unstable toward the superoxide⁵⁷ but to a certain extent are stable against peroxides.⁵⁸ Meanwhile, PVP and PEO contain EDGs on side chains or within the polymer backbone while PMMA contains both EDGs (-CH₃) and EWGs (-COOCH₃) on its side chain. These different structures and chemical moieties can be very helpful in addressing the different aspects of the binder effect on SABs. In our previous study²⁷ we showed that when using pure oxygen as the gas source, CNT-PVDF air electrodes exhibit electrochemical charge-discharge profiles similar to other studies reporting NaO₂ as the primary discharge product. However, it showed the coexistence of NaO₂ and Na₂O₂ in the discharge product when cycled in dry air.²⁷ Herein, dry air is chosen as a gas source instead of pure oxygen in order to (i) acquire general information on the influence of both superoxide O₂⁻ and peroxide O₂²⁻ species on the polymer binders and (ii) attempt to simulate the practical environment of the usage of SABs.

Cyclic voltammetry measurements

CV measurements have been firstly carried out on the SABs with the four different binders and the results are shown in Fig. 1. Clearly, the four cells demonstrate very different electrochemical

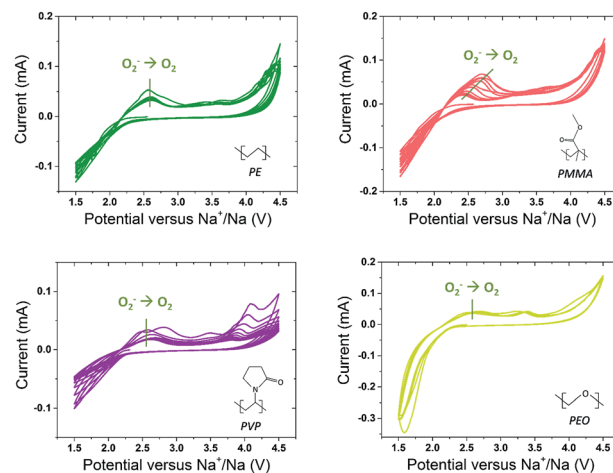


Fig. 1 The CV curves of the air electrodes with PE, PMMA, PVP and PEO binders.

responses during the tests. The first and subsequent cycle CV curves of the SAB with a PE binder are found to be very similar except for the gradual degradations in current densities. Although no obvious current peak can be found for cathodic scans for the SAB with a PE binder, the major anodic current peaks that locate at around 2.60 V can be observed for all the CV cycles, which is consistent with the electrochemical decomposition of NaO₂.^{17,24,35,82} Besides, some weak anodic current peaks at 3.63 and 3.40 V can be observed in the CV curves of the initial two cycles, implying that some irreversible side reaction had occurred.

In contrast, the first anodic scan of the SAB with a PMMA binder shows one strong current peak at 2.55 V, which gradually shifts to lower potentials (2.42 V at the 10th cycle). The area of this series of the anodic peaks as well as the cathodic peaks also rapidly decayed during the first 10 cycles. Meanwhile, another anodic current peak appeared at 3.38 V since the 4th cycle. The decreased polarizations of the anodic current peaks may be attributed to various possible reasons, including (i) the increased H⁺/H₂O concentration as the result of the decomposition of the PMMA in the presence of superoxide and (ii) the decreased amount of reduction product as evidenced from the shrunk area of the cathodic peak in the subsequent cycles.

Regarding the SAB with a PVP binder, which is known to be unstable to both superoxides and peroxides, a CV curve is shown with more complicated features, indicating an apparent influence of binder on the electrochemical response of SABs. The intensity of the cathodic current peaks is also observed to drop fast during subsequent CV cycles. Meanwhile, four anodic current peaks at 2.49 V, 2.81 V, 3.49 V, and 4.09 V are observed in the 1st cycle. The appearance of four anodic current peaks had been also observed in our previous study on the effect of relative humidity (RH) on SABs,⁶¹ which suggests an increased water concentration. However, only two groups of anodic current peaks appear in all the following cycles, one of which is located at around 2.60 V while the other shifts from 4.05 V to 3.81 V from the 2nd to 10th scan. The trend that the CV curves of SABs with PMMA and PVP seem to stabilize after several scans may be attributed to the assumption of a passivation effect

proposed by Nasybulin *et al.*,⁵⁷ who suggest that a stable passive layer can deposit on the unstable binders upon initial contact with superoxide/peroxide ions.

When PEO is used as a binder for SABs, it is interesting to note that only a single obvious cathodic current peak is observed at around 1.58 V. However, two current peaks around 2.60 V and 3.36 V are found in all subsequent anodic scans. The relative overlapping of CV cycles in the SAB with PEO implies a highly reversible redox process in the cell.

A general comparison on the current densities can be also made among the SABs using four different binders. It can be observed that the SABs with PE, PVP and PMMA binders exhibited relatively close initial cathodic peak current densities, while the SAB with a PEO binder showed much increased current density. Such differences may be related to the kinetic factor, the reaction mechanism, and/or the altered proton/water concentration due to the possible side reaction(s) between the binder and discharge products. In contrast, the current densities of the first anodic peaks of the SABs with PE, PVP and PMMA binders are found to be of a very similar proportion (approximately half in value) to those of the corresponding cathodic peaks. However, the corresponding value of the SAB with a PEO binder is found to be much reduced, which implies the alternated reaction mechanism as discussed above.

Overall, the CV tests clearly show the different electrochemical responses of SABs with various binders. As indicated by their CV curves, the polymer binders have a significant impact on the electrochemical behaviour of SABs.

Cycling performance

Afterwards, examinations of charge and discharge curves were carried out to understand the influence of the binders on the cycling performance of SABs. Two cycling modes have been chosen in this study: one is the full discharge and charge cycling between 1.5 and 4.5 V (deep cycling); the other is the limited discharge and charge cycling mode with a cut-off capacity of 300 mA h g_{carbon}⁻¹ (shallow cycling).

In order to give a convenient comparison, the charge/discharge curves are divided into three regions, *i.e.* 2.25–2.75 V (region A), 2.75–3.5 V (region B), and 3.5–4.5 V (region C), which are also marked with three colors in Fig. 2. Based on a general summary from previously published results, it can be inferred that SABs with different types of discharge products possess identifiable features in the shapes of their charge curves:

(i) When NaO₂ is the major discharge product, the charge curves are composed of only one voltage plateau in region (A) when cycled with enough proton donors in the cell;^{17,19,21,23,24}

(ii) However, when cycled in the electrolyte with 0 ppm water (or any other proton donor), the charging curve of the cell with NaO₂ discharge product alternatively shows a short spike in region (B) followed by two voltage plateaus in regions (A) and (C);²³

(iii) For the SAB cells with Na₂CO₃ as the major discharge product, generally only one voltage slope/plateau in region (C) can be observed;^{34,82}

(iv) For the SABs with Na₂O₂·2H₂O as the final product (which may be produced by the chemical reactions between

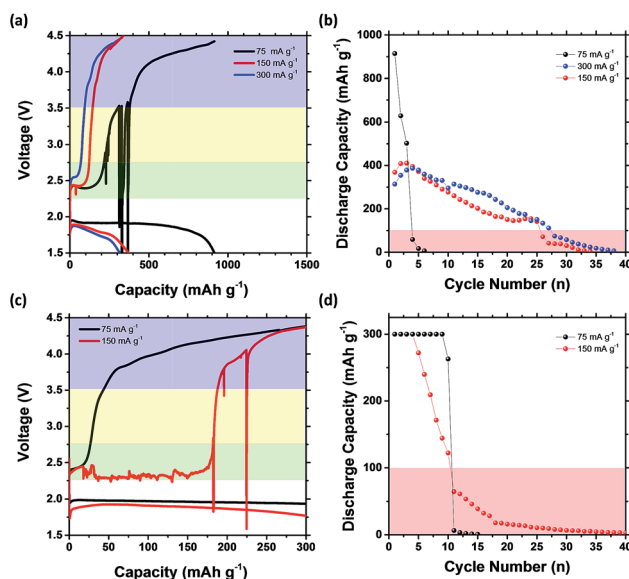


Fig. 2 (a) First charge and discharge curves of CNT-PE air electrodes at 75, 150, and 300 mA g⁻¹, (b) cycling retentions in voltage-limited cycling mode; (c) first charge and discharge curves at 75 and 150 mA g⁻¹ and (d) cycling retentions in capacity-limited cycling mode of the air electrode with a PE binder. The green, yellow, and purple areas in (a) and (c) represent regions (A), (B), and (C), respectively.

sodium superoxide/peroxide and water), typically three voltage plateaus respectively in regions (A), (B), and (C) are found in the charge process;^{21,30,35,88}

(v) For the SABs with NaOH as another side product from the contamination of water, the charge curves shows plateaus in region (B);^{24,61,82}

(vi) Finally, for the SABs with mixed discharge products, *e.g.* NaO₂ + Na₂O₂ (ref. 31, 32 and 40) or Na₂O₂ + Na₂CO₃,^{25,31} these cells often demonstrate charge curves composed of combined several plateaus/slopes in the same corresponding region as each of the respective component.

Therefore, it can, accordingly, be able to identify the components inside the discharge products from the shape of the charge curves of SABs. On grounds of the above discussion, the discharge and charge curves of the SABs with different binders can be analyzed in detail.

PE

The PE binder is expected to be stable against NaO₂ and Na₂O₂. All of the discharge curves of the SABs with a PE binder cycled in the voltage range of 1.5 to 4.0 V (deep cycling mode) at the constant current densities of 75, 150, and 300 mA g⁻¹ demonstrate a combination of two voltage plateaus as shown in Fig. 2(a) (1.95 and 1.91 V at 75 mA g⁻¹, 1.88 and 1.78 V at 150 mA g⁻¹, and 1.86 and 1.71 V at 300 mA g⁻¹). Meanwhile, all three first charge curves at the same current densities are composed of one charge plateau in region (A) and two in region (C). The absence of charge capacities in region (B) indicates that almost no Na₂O₂·2H₂O or NaOH exists in the discharge product, implying negligible water should have formed during the cycling of the cell. Therefore, region (A) in the curves for the

cells with PE binders should be accordingly assigned to the decomposition of NaO_2 , while region (C) should be related to Na_2CO_3 and/or Na_2O_2 . Consequently, the discharge capacities of CNT-PE air electrodes are rather low, which is consistent with Nazar's²³ and our⁶¹ previous work showing decreased capacity with a reduced amount of H_2O in the cell. Meanwhile, an increasing overpotential in region (A) for increased current densities can be observed, which is consistent with previous reports where NaO_2 is found to be the sole discharge product.^{17,21}

The cycling stability of the CNT-PE air electrode at a low current density of 75 mA g^{-1} is very poor, which rapidly decays in 5 cycles (Fig. 2(b)). In contrast, the CNT-PE air electrodes cycled at current densities of 150 and 300 mA g^{-1} show very similar capacity retention trends. Considering the significant difference in capacities for the CNT air electrodes with various binders, we adopt a capacity of 100 mA h g^{-1} to indicate the termination cycle lives of cells as a general comparison. The gradual decrease in the discharge capacity of CNT-PE air electrodes cycled at 150 mA g^{-1} and 300 mA g^{-1} implies that the failure of the cells may be attributed to the incomplete removal of discharge products. This observation can be also supported by the relatively low coulombic efficiencies of the two cells ($\sim 91\%$ for 150 mA g^{-1} and $\sim 77\%$ for 300 mA g^{-1} in average for the first 25 cycles, respectively).

To further investigate the influence of binders on the electrochemical performance, cycling stability, and reaction mechanisms of SABs, a capacity-limited charge and discharge measurement (shallow cycling mode) with a cut-off capacity of 300 mA h g^{-1} has been carried out with the results shown in Fig. 2(c) and (d). The cell with a CNT-PE air electrode cycled at 75 mA g^{-1} with this cut-off capacity exhibited a very similar charge-discharge curve to the cell cycled in the deep cycling mode. However, the curve of the cell cycled at 75 mA g^{-1} showed a completely different feature: a long and highly unsteady voltage plateau has been found in region (A); after this voltage range, the charge curve continued with two voltage slopes in region (C). A possible explanation for this unsteady section of the charge curve herein may be due to the sodium anode as the result of dendrite growth,²² and/or attack by dissolved superoxide species,³⁵ and/or increased H_2O concentration introduced by the decomposition of byproducts.⁶¹ Similar sudden voltage drops have been also witnessed by Bi *et al.*,²² while they have shown that such voltage drops can be eliminated when an ion selective membrane (Nafion- Na^+ membrane) is adopted instead of a conventional glass-fiber separator. Meanwhile, the absence of plateaus in region (B) in the charge curves of CNT-PE cells in the shallow cycling mode also indicates a lack of $\text{Na}_2\text{O}_2 \cdot 2\text{H}_2\text{O}/\text{NaOH}$. Therefore, it can be assumed that region (A) for both cells should be assigned to the electrochemical removal of superoxide. The obvious prolonged charge capacity at low voltage at 150 mA g^{-1} is also consistent with the observations of other types of air electrodes previously reported by our group.³⁰ However, the cycle lives of the both CNT-PE cells cycled at 75 and 150 mA g^{-1} are still very poor (around 10 cycles). Compared to the deep cycling mode, the shallow cycled CNT-PE cell at 75 mA g^{-1} shows an improved stability, which supports the aforementioned

assumption that the failure of the cell may be related to the incomplete removal of the discharge product. In contrast, the shallow cycled CNT-PE cell at 150 mA g^{-1} shows even faster decaying than that in the full cycling mode, which is unexpected. The reason behind this may be attributed to the apparent difference in charge behaviour as shown in the charge curves. A more detailed analysis will be given in the following sections.

PMMA

When moving to PMMA as the binder for CNT air electrodes, an overwhelming increase in discharge capacity of 3417, 4546, and 3871 mA h g^{-1} can be achieved for current densities of 75, 150, and 300 mA g^{-1} , respectively (Fig. 3(a)). However, the cells rapidly fail within a few cycles (Fig. 3(b)), which is also consistent with the fast dropping current peaks in the CV curves of the CNT-PMMA air electrode. The discharge and charge curves of the CNT-PMMA air electrode cycled at 75 mA g^{-1} contain a short slope in region (B) and two slopes in region (C) (Fig. 3(c)), while its initial coulombic efficiency is only around 41%. Meanwhile, the corresponding discharge and charge curves of the CNT-PMMA air electrode cycled at 150 and 300 mA g^{-1} contain three plateaus/slopes in region (A), (B), and (C) (Fig. 3(d)). They also show very similar curve features in spite of the increased polarization as the result of a higher current density, while their initial coulombic efficiencies reach 95% and 94% when cycled at 150 and 300 mA g^{-1} , respectively.

As discussed above, the existence of a voltage slope in region (B) implies the decomposition of NaOH at the air electrode. Additionally, taking into consideration the significant discharge capacities of the cells, it can be inferred that notable amounts of water or other proton donors^{42,61} should have been formed during the discharge process, which is likely to be a result of the

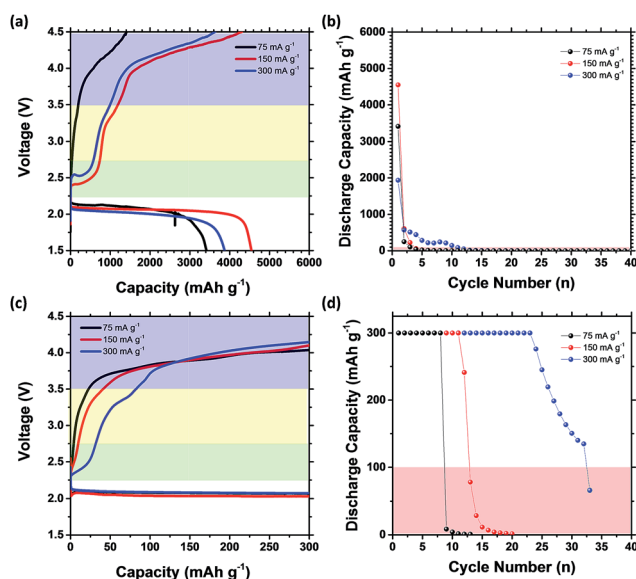


Fig. 3 (a) First charge and discharge curves of CNT-PMMA air electrodes at 75, 150, and 300 mA g^{-1} , (b) cycling retentions in voltage-limited cycling mode; (c) first charge and discharge curves at 75 and 150 mA g^{-1} and (d) cycling retentions in capacity-limited cycling mode of the air electrode with a PMMA binder.

side reactions between superoxide O_2^- and the PMMA polymer, since PMMA is reported to be relatively stable against peroxide species.⁵⁸ As discussed by Amanchukwu *et al.*,⁵⁸ the absence of α -H in PMMA enhances its backbone chain stability. Therefore, it is reasonable to expect a nucleophilic addition/substitution reaction at the carbonyl site.⁷¹ According to this reaction mechanism, the continuous consumption of dissolved O_2^- in the electrolyte can result in a reduced concentration of O_2^- in electrolyte solvent and promote the reversible dissolution of NaO_2 ,⁸⁹ which further contributes to the large capacity of the SAB cell with a CNT-PMMA air electrode. This mechanism is also consistent with the observation that almost no capacity from region (A) can be found in the charge curve of the cells with the CNT-PMMA air electrode cycled at 75 mA g^{-1} (Fig. 3(a)), which should be related to the nearly complete decomposition of NaO_2 during the extended discharge period. In contrast, the charge curves of the cells with the CNT-PMMA air electrode cycled at 150 and 300 mA g^{-1} show features typical of SABs in which $Na_2O_2 \cdot 2H_2O$ is reported to form as the discharge product.^{30,90} We attribute this phenomenon to the higher rate of O_2^- production at high current densities. Because the reaction rate between PMMA and O_2^- should be limited by kinetics, the dissolved O_2^- with increasing concentration or participant NaO_2 is likely to either react with ether solvent resulting in $Na_2O_2 \cdot 2H_2O$ (ref. 36 and 89) or decompose PMMA *via* an alternative reaction route to deliver H_2O , which may further react with NaO_2/Na_2O_2 to form $Na_2O_2 \cdot 2H_2O$. Taking the following facts into consideration that (a) the weak but still increased β -H acidity in the main chain of PMMA as the β -C atom is conjoined to two α -C atoms that connect to the strong EWG, and (b) the strong H-abstraction tendency of the superoxide to form organic radicals, and assuming a decomposition mechanism analogous to those of ethers/dimethyl sulfoxide electrolyte against superoxide species,^{76,91–93} we can accordingly propose another possible reaction route between PMMA and O_2^- as shown in Scheme S1.†

In order to verify the proposed reaction mechanism and further probe the cycling performance of CNT-PMMA air electrodes, capacity-limited charge and discharge mode measurements have been also carried out with a cut-off capacity of 300 mA h g^{-1} with the results displayed in Fig. 3(c) and (d). It can be observed that the discharge curves of the cells with CNT-PMMA air electrodes at current densities of 75, 150, and 300 mA g^{-1} are nearly overlapping due to the small proportion of the discharge capacity relative to the significantly higher full discharge capacity of these air electrodes. The cells cycled at 75 and 300 mA g^{-1} show charge curves with features similar to the corresponding cells in the full discharge/charge mode. Interestingly, the cell cycled at 150 mA g^{-1} shows a reduced charge capacity in regions (A) and (B), implying a decreased proportion of the $Na_2O_2 \cdot 2H_2O$ product. This phenomenon is consistent with the above assumption that $Na_2O_2 \cdot 2H_2O$ is a result of the side reactions involving an increased amount of O_2^- . In terms of cycling stability, it can be seen that significantly longer cycle lives can be achieved for the capacity-limited cycling of the cells (Fig. 3(d)) in spite of the rapid decay in a voltage-limited mode. This can be attributed to the large overall capacity of the air electrodes with PMMA binders and

prevention of forming excess discharge products, which are difficult to decompose during charging.

PVP

Afterwards, we picked up PVP as the binder for CNT air electrodes. PVP has been known to be unstable toward both superoxide and peroxide species.^{57,58} This is consistent with the CV curves of CNT-PVP air electrodes as discussed above. Interestingly, the main chain of the PVP polymer links to an EDG, which should not be favorable to promote the reaction with superoxide/peroxide. Therefore, the reaction sites between PVP and O_2^-/O_2^{2-} have been believed to be within the side chain, *i.e.* the lone pair electrons in N, the carbonyl $C=O$ group and its α -H.^{58,93} From the discharge and charge curves of the CNT-PVP air electrodes (Fig. 4(a)), it can be found that their discharge capacities at all three current densities are still relatively large, which are much higher than those with PE binders but still lower than those with PMMA binders. This can also be consistent with the known reactivity between PVP and both peroxide/superoxide.^{57,58} The charge curves of CNT-PVP air electrodes at 75 and 150 mA g^{-1} clearly combine different stages from all regions (A), (B), and (C), undoubtedly indicting the formation of $Na_2O_2 \cdot 2H_2O$. For the CNT-PVP air electrode cycle at 300 mA g^{-1} , a very noisy quasi-voltage plateau is observed, which may have resulted from the increased water content in the electrolyte as shown in our previous work on the humidity effect on SABs⁶¹ and/or Na dendrite formation at this high current density, which is similar to what had been observed by Bi *et al.*²² Unsurprisingly, the cycling retentions of the SABs with PVP binders are found to be very poor (Fig. 4(b)). Nonetheless, in the capacity-limited cycling

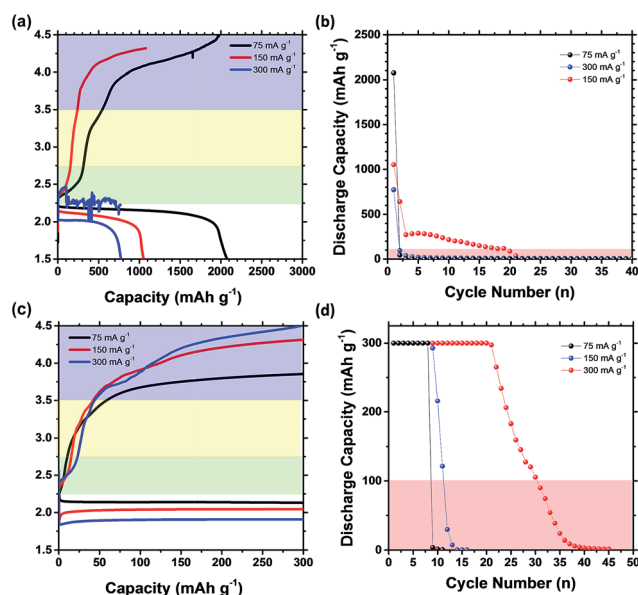


Fig. 4 (a) First charge and discharge curves of CNT-PVP air electrodes at 75, 150, and 300 mA g^{-1} , (b) cycling retentions at voltage-limited cycling mode; (c) first charge and discharge curves at 75 and 150 mA g^{-1} and (d) cycling retentions in capacity-limited cycling mode of the air electrode with a PVP binder. The green, yellow, and purple areas in (a) and (c) represent regions (A), (B), and (C), respectively.

mode, the SABs with PVP binders show improved stabilities, although nearly no capacity can be found in region (A), while more capacities are presented in region (B), more likely to suggest the existence of a NaOH phase (Fig. 4(c)). Meanwhile, the cycling retention of these cells with a 300 mA h g^{-1} limitation also seems to be much improved (Fig. 4(d)). This may be explained by a previous study by Amanchukwu *et al.*,⁵⁸ who suggest that the PVP's reaction with Li_2O_2 is a slow reaction. In contrast, considering the diminished charge capacity in region (A) for all the CNT-PVP air electrodes, it may be assumed that the reaction between PVP and Na_2O_2 should be relatively fast. The possible reaction mechanisms between PVP and O_2^- are accordingly suggested to follow the mechanisms shown in Scheme S2.†

PEO

Finally, the employment of a PEO binder in SABs is discussed. It has been reported that PEO is stable against Li_2O_2 with the exception of some cross-linking reactions;⁵⁸ however, mixing of KO_2 with PEO resulted in K_2CO_3 and other unidentified product(s).⁵⁷ Experimentally, as inferred from its CV curves shown above, the CNT-PEO air electrode seems to deliver a relatively stable electrochemical response. The discharge-charge curves of SABs with CNT-PEO air electrodes at 75, 150, and 300 mA g^{-1} all show a combination of one voltage plateau around 2.4 V in region (A) and three sloped voltage plateaus in region (C) in the voltage-limited cycling mode (Fig. 5(a)), while similar features can be also observed in the capacity-limited cycling mode (Fig. 5(b)). Similar to the PE binder, the fact that negligible capacity can be found in region (B) indicates that PEO should be relatively stable against the superoxide/peroxide formed during discharge. However, the discharge capacity of the cell cycled at 75 mA g^{-1} compared to those cycled at 150 and 300 mA g^{-1} (Fig. 5(c)) demonstrates that

the PEO binder is still partially decomposed under the attack of O_2^- , which should be limited by a slow kinetics process. This is consistent with the sluggish reactivity between ether solvent and superoxides in metal-air batteries, considering the structural similarity between PEO and ether solvents. It has also been reported that PEO suffers from more severe decomposition when charging in the presence of O_2 than under Ar,⁵⁹ which can explain the poor cycling performance of the CNT-PEO air electrodes at all current densities and in both voltage- and capacity-limited cycling modes (Fig. 5(c) and (d)).

The chemical reaction mechanism between PEO and the superoxide radical O_2^- is expected to be similar to the decomposition route of ethers against O_2^- as proposed in previous ref. 37, 76 and 93 and is depicted in Scheme S3(a).† Meanwhile, in order to address the electrochemical decomposition mechanism of PEO, we can take notes from (1) the cross-linking of PEO in the presence of Li_2O_2 ,⁵⁸ (2) the increased consumption of O_2 by PEO in the cells at higher potentials,⁵⁹ (3) the hopping mechanism of Li^+/Na^+ transportation in PEO-based polymer electrolyte (Li^+/Na^+ coordinating to oxygen in PEO),⁹⁴ (4) the possible reaction tendency of H abstraction from polyether by O_2^- to form organic radicals,⁷⁶ and (5) the $\text{S}_{\text{N}}2$ reactions of O_2^- .⁷¹ Accordingly, it can be proposed that PEO decomposes through an electrochemically driven decomposition mechanism with a free-radical mediated reaction route as shown in Scheme S3(b).†

Physical characterization

More information may be further achieved by comparing the SEM images of the initial, discharged, and charged states of the air electrodes with different binders as shown in Fig. 6. The order

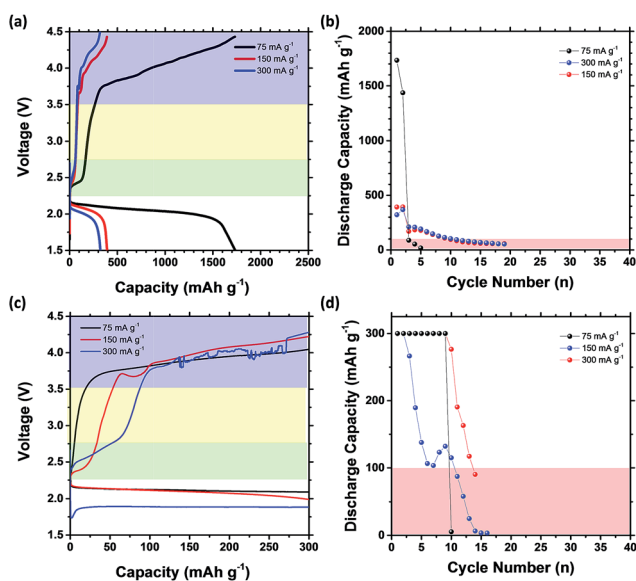


Fig. 5 (a) First charge and discharge curves of CNT-PEO air electrodes at 75, 150, and 300 mA g^{-1} , (b) cycling retentions in voltage-limited cycling mode; (c) first charge and discharge curves at 75 and 150 mA g^{-1} and (d) cycling retentions in capacity-limited cycling mode of the air electrode with a PEO binder.

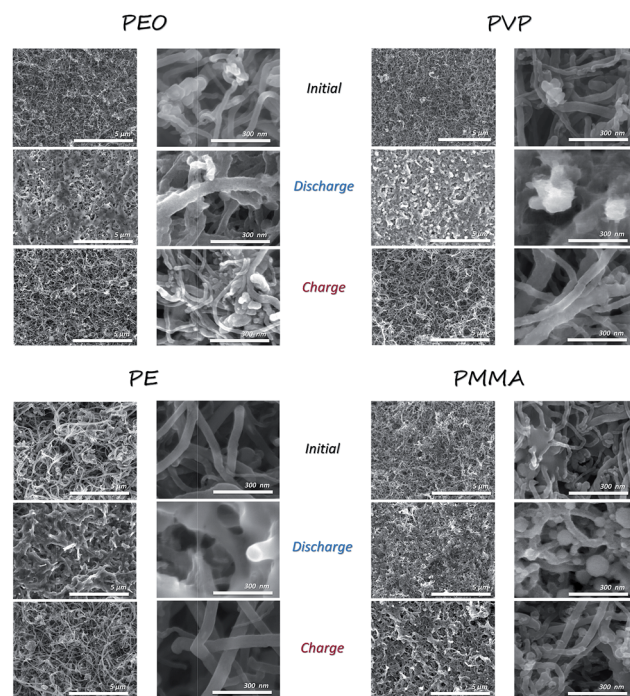


Fig. 6 SEM pictures of the initial, 1st fully discharged, and 1st fully charged air electrodes with PE, PMMA, PVP and PEO binders at the current of 150 mA g^{-1} .

of the SEM images from left to right is also ranked by the strength of the EDG/EWG as shown in Fig. 8. It can be observed that discharged CNT-PE and CNT-PEO air electrodes show very similar morphologies as previously observed on CNT-PVDF air electrodes,³² and are composed of layer-like discharge products on the electrode surface. After recharging, the morphologies of CNT-PE and CNT-PEO air electrodes recover well. In contrast, the discharge product of the CNT-PVP air electrode seems to be more dense and adherent to the CNTs. The large amount of discharge product of the CNT-PVP air electrode is also consistent with its larger discharge capacity. Meanwhile, some residual substances can also be observed on the surface of CNTs after recharging, indicating an incomplete removal of the discharge product. Finally, it is very interesting to find a large quantity of particles in sphere-like or round-corner cubic shapes on the surface of the discharged CNT-PMMA air electrodes. Meanwhile, the PMMA polymers appear to be decomposed based on the SEM images of the charged air electrode.

Moreover, XRD and FT-IR characterizations have been also carried out to examine the initial and discharged air electrodes to detect discharge and side products. By comparing the XRD pattern of the initial and discharged air electrodes, it can be clearly found that the CNT-PEO and CNT-PVP air electrodes exhibited diffraction peaks corresponding to NaOH·H₂O (JCPDS 30-1194) and Na₂CO₃ (JCPDS 77-2082) after discharge. Meanwhile, sodium methylate CH₃ONa (JCPDS 19-1876) is found to exist in the discharged CNT-PMMA air electrode, which can be consistent with the totally different shape of the discharge product of the CNT-PMMA air electrode compared to other air electrodes from the SEM pictures (Fig. 6). In contrast, no signal corresponding to any side products can be found in the same angle range of the XRD pattern of the discharged CNT-PE air electrode, implying a much reduced side product formation when PE is used as the binder. These XRD results are of great consistency with the above electrochemical behavior of the SABS with the four binders. Meanwhile, from the FT-IR

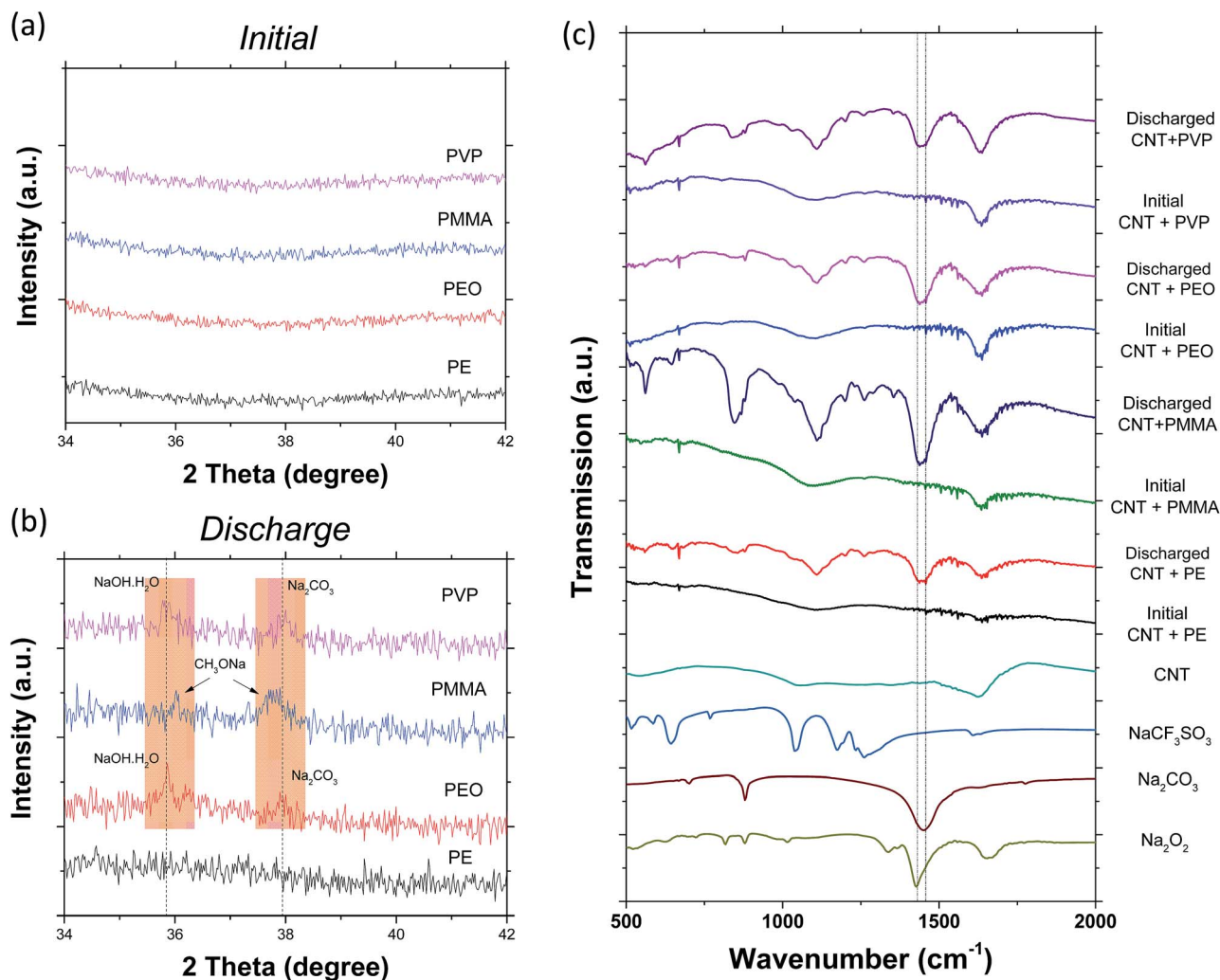


Fig. 7 XRD pattern of the (a) initial and (b) 1st fully discharged CNT air electrodes with PE, PMMA, PVP and PEO binders at the current of 150 mA g⁻¹; (c) FT-IR spectra of the initial and 1st fully discharged CNT air electrodes with PE, PMMA, PVP and PEO binders at the current of 150 mA g⁻¹; the FT-IR spectra of the pristine CNT powder and standard samples of electrolyte salt, Na₂CO₃ and Na₂O₂ are also shown for comparison.

results and comparing the standard spectra of Na_2O_2 , Na_2CO_3 , electrolyte salt (NaCF_3SO_3) and pristine CNT, it can be concluded that sodium peroxide has been detected as the discharge product of the full discharged SABs with all four binders. Nonetheless, a certain amount of Na_2CO_3 is also found for the all four discharged air electrodes according to the FT-IR results, implying that amorphous sodium carbonate has formed in the discharged CNT-PE air electrode which was not detected by the XRD results. Overall, the XRD and FT-IR results indicate that the determined discharge products of the SABs using different binders are in good agreement with their electrochemical performance as discussed above.

Comparison and discussion

After the above detailed descriptions and analysis on the electrochemical behaviour of SABs using different polymer binders, an overall comparison on their impacts can be made in order to summarize the general influence of binders on SABs. In order to make a conventional comparison, the key parameters (capacity and cycle life) of the SABs with different binders are summarized in Fig. 7. The electrochemical data for a SAB with CNT-PVDF air electrode taken from our previous studies^{32,61} are also included for comparison. Obviously, the introduction of a strong EWG in PMMA leads to the activation of $\beta\text{-H}$ as the proton source for H_2O or HO_2 and results in the significantly increased capacity. Meanwhile, although the main chain of PVP is linked to the N atom as an EDG, the $\alpha\text{-H}$ in its side chains should also play a similar role and thus enhance the capacities. Although the air electrodes with a PEO binder may be relatively unstable at low current densities and long exposure time to O_2^- , they deliver a larger capacity than the corresponding cell with PE. The capacities of CNT-PEO and CNT-PE air electrodes nearly overlap at high current densities, indicating an improved stability. In terms of capacity retention, PE, as the most stable polymer in this study, undoubtedly exhibits the longest cycle life in voltage- and capacity-limited modes. Nevertheless, the air electrodes with a PVDF binder also exhibit long cycle lives in SABs, similar to those with a PE binder, which is consistent with a previous study³⁷ on LABs. However, benefiting from the large full discharge/charge capacity, the air electrodes with PEO, PVP, and PMMA binders along with EDGs/EWGs still deliver comparable cycling performance in the capacity-limited mode, exhibiting much longer cycle lives than the cells with the same binders cycled in voltage-limited mode, especially at a high current density of 300 mA g^{-1} . This phenomenon may be due to the shorter exposure time of polymers to O_2^- before charging.

Clearly, it has been shown in this study that the binder can play an important role in SABs based on the observed electrochemical results. The binders not only significantly influence the discharge-charge curves and capacities of the SABs, but also result in different discharge product morphologies. The existence of EDGs/EWGs in the polymer can be the key to the understanding of the electrochemical behaviour of these polymers in the presence of O_2^- and O_2^{2-} . The reaction mechanisms can be deduced from the analysis of the voltage ranges of charge curves as well as the known chemical stabilities and

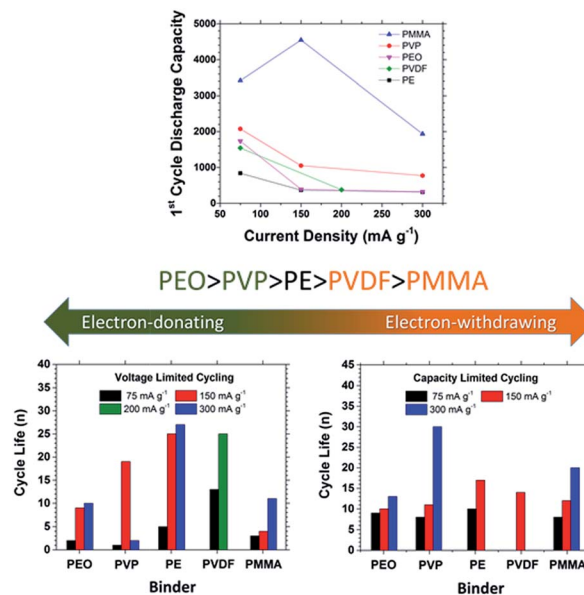


Fig. 8 The overall comparison of the first cycle discharge capacities and cycle lives of the air electrode with PE, PMMA, PVP and PEO binders in both voltage-limited and capacity-limited cycling modes, respectively.

possible chemical decomposition products from ref. 57–59, which has also been supported by the physical characterization results in this study. Combining all the achieved data and the inferred conclusion in this study, EWGs either in the main chain of the polymer (PEO), or as a side chain linked to the main chain (PMMA), or confined in the side chain of the polymer (PVP) can be responsible to the increased side reactions when they are used as the binder for sodium-air batteries (SABs). Therefore, three types of polymer binders are expected to be the most stable choices for future SABs: (i) the polymer without any additional functional groups, *i.e.* PE; (ii) the polymers with no EWGs in either their main or side chains, such as alkyl groups (*e.g.* polypropylene (PP), polyisobutylene (PIB), and polybutene (PB) *etc.*); and (iii) perfluorinated polymers such as polytetrafluoroethylene (PTFE). We believe that the presented study along with the above-mentioned previous studies on the electrochemical/chemical (in) stabilities of polymer binders against superoxide/peroxide species can provide further insight on the impact of binders on SAB performance, ultimately leading toward their rational design as well as contributing to the future target of precise control over discharge products.

Conclusions

In summary, the role of different polymer binders with (or without) different functional groups is investigated in SABs. It has been shown that the choice of binder can significantly influence the electrochemical response and long-term durability of SABs. On one hand, the introduction of a stable PE binder enables an improved stability of the air electrode against O_2^- and O_2^{2-} , resulting in longer cycle lives. On the other hand, the existence of EWGs linked to either main or side chains

result in the activation of α/β -H and their increased acidity. This leads to increased capacities but poorer cycling stabilities. Meanwhile, the reactions between O_2^-/O_2^{2-} and polymer binders are still kinetics limited, thus, the cells with binders unstable towards these reactants may still exhibit long cycle lives by charging at high current densities and limited discharge capacities. This is a result of quickly reducing the concentration of superoxide species in electrolyte. In addition, the reaction mechanisms between different binders with O_2^- have been also proposed accordingly. Thus, it can be concluded that the role of the binder is complex, and this work can be used as a basis for future rational design of SABs.

Conflicts of interest

There are no conflicts to declare.

Acknowledgements

This research was supported by the Natural Science and Engineering Research Council of Canada (NSERC), the Canada Research Chair Program (CRC), the Canada Foundation for Innovation (CFI), and the University of Western Ontario (UWO).

Notes and references

- B. L. Ellis and L. F. Nazar, *Curr. Opin. Solid State Mater. Sci.*, 2012, **16**, 168–177.
- E. Peled, D. Golodnitsky, R. Hadar, H. Mazor, M. Goor and L. Burstein, *J. Power Sources*, 2013, **244**, 771–776.
- S. Ha, J.-K. Kim, A. Choi, Y. Kim and K. T. Lee, *ChemPhysChem*, 2014, **15**, 1971–1982.
- S. K. Das, S. Lau and L. A. Archer, *J. Mater. Chem.*, 2014, **2**, 12623–12629.
- P. Adelhelm, P. Hartmann, C. L. Bender, M. Busche, C. Eufinger and J. Janek, *Beilstein J. Nanotechnol.*, 2015, **6**, 1016–1055.
- H. Yadegari, Q. Sun and X. Sun, *Adv. Mater.*, 2016, **28**, 7065–7093.
- W.-W. Yin and Z.-W. Fu, *ChemCatChem*, 2016, **9**, 1545.
- I. Landa-Medrano, C. Li, N. Ortiz-Vitoriano, I. R. de Larramendi, J. Carrasco and T. Rojo, *J. Phys. Chem. Lett.*, 2016, **7**, 1161–1166.
- A. C. Luntz and B. D. McCloskey, *Chem. Rev.*, 2014, **114**, 11721–11750.
- P. G. Bruce, S. A. Freunberger, L. J. Hardwick and J.-M. Tarascon, *Nat. Mater.*, 2011, **11**, 19–29.
- J. Wang, Y. Li and X. Sun, *Nano Energy*, 2013, **2**, 443–467.
- J. Lu, L. Li, J.-B. Park, Y.-K. Sun, F. Wu and K. Amine, *Chem. Rev.*, 2014, **114**, 5611–5640.
- X. Ren and Y. Wu, *J. Am. Chem. Soc.*, 2013, **135**, 2923–2926.
- X. Ren, K. C. Lau, M. Yu, X. Bi, E. Kreidler, L. A. Curtiss and Y. Wu, *ACS Appl. Mater. Interfaces*, 2014, **6**, 19299–19307.
- X. Ren, M. He, N. Xiao, W. D. McCulloch and Y. Wu, *Adv. Energy Mater.*, 2017, **7**, 1601080.
- J. Lu, L. Li, J.-B. Park, Y.-K. Sun, F. Wu and K. Amine, *Chem. Rev.*, 2014, **114**, 5611–5640.
- P. Hartmann, C. L. Bender, M. Vračar, A. K. Dürr, A. Garsuch, J. Janek and P. Adelhelm, *Nat. Mater.*, 2013, **12**, 228–232.
- P. Hartmann, C. L. Bender, J. Sann, A. K. Dürr, M. Jansen, J. Janek and P. Adelhelm, *Phys. Chem. Chem. Phys.*, 2013, **15**, 11661–11672.
- C. L. Bender, P. Hartmann, M. Vračar, P. Adelhelm and J. Janek, *Adv. Energy Mater.*, 2014, **4**, 1301863.
- I. I. Abate, L. E. Thompson, H.-C. Kim and N. B. Aetukuri, *J. Phys. Chem. Lett.*, 2016, **7**, 2164–2169.
- N. Ortiz-Vitoriano, T. P. Batcho, D. G. Kwabi, B. Han, N. Pour, K. P. C. Yao, C. V. Thompson and Y. Shao-Horn, *J. Phys. Chem. Lett.*, 2015, **6**, 2636–2643.
- X. Bi, X. Ren, Z. Huang, M. Yu, E. Kreidler and Y. Wu, *Chem. Commun.*, 2015, **51**, 7665–7668.
- C. Xia, R. Black, R. Fernandes, B. Adams and L. F. Nazar, *Nat. Chem.*, 2015, **7**, 496–501.
- N. Zhao, C. Li and X. Guo, *Phys. Chem. Chem. Phys.*, 2014, **16**, 15646–15652.
- Q. Sun, Y. Yang and Z.-W. Fu, *Electrochem. Commun.*, 2012, **16**, 22–25.
- W. Liu, Q. Sun, Y. Yang, J.-Y. Xie and Z.-W. Fu, *Chem. Commun.*, 2013, **49**, 1951–1953.
- W.-M. Liu, W.-W. Yin, F. Ding, L. Sang and Z.-W. Fu, *Electrochem. Commun.*, 2014, **45**, 87–90.
- J. Kim, H.-D. Lim, H. Gwon and K. Kang, *Phys. Chem. Chem. Phys.*, 2013, **15**, 3623–3629.
- Y. Li, H. Yadegari, X. Li, M. N. Banis, R. Li and X. Sun, *Chem. Commun.*, 2013, **49**, 11731–11733.
- H. Yadegari, Y. Li, M. N. Banis, X. Li, B. Wang, Q. Sun, R. Li, T.-K. Sham, X. Cui and X. Sun, *Energy Environ. Sci.*, 2014, **7**, 3747–3757.
- Y. Hu, X. Han, Q. Zhao, J. Du, F. Cheng and J. Chen, *J. Mater. Chem. A*, 2015, **3**, 3320–3324.
- Q. Sun, H. Yadegari, M. N. Banis, J. Liu, B. Xiao, B. Wang, S. Lawes, X. Li, R. Li and X. Sun, *Nano Energy*, 2015, **12**, 698–708.
- W.-J. Kwak, Z. Chen, C. S. Yoon, J.-K. Lee, K. Amine and Y.-K. Sun, *Nano Energy*, 2015, **12**, 123–130.
- S. Zhang, Z. Wen, K. Rui, C. Shen, Y. Lu and J. Yang, *J. Mater. Chem. A*, 2015, **3**, 2568–2571.
- J. Kim, H. Park, B. Lee, W. M. Seong, H.-D. Lim, Y. Bae, H. Kim, W. K. Kim, K. H. Ryu and K. Kang, *Nat. Commun.*, 2016, **7**, 10670.
- S. Y. Sayed, K. P. C. Yao, D. G. Kwabi, T. P. Batcho, C. V. Amanchukwu, S. Feng, C. V. Thompson and Y. Shao-Horn, *Chem. Commun.*, 2016, **52**, 9691–9694.
- R. Black, A. Shyamsunder, P. Adeli, D. Kundu, G. K. Murphy and L. F. Nazar, *ChemSusChem*, 2016, **9**, 1795–1803.
- I. M. Aldous and L. J. Hardwick, *Angew. Chem., Int. Ed.*, 2016, **55**, 8254–8257.
- B. Wang, N. Zhao, Y. Wang, W. Zhang, W. Lu, X. Guo and J. Liu, *Phys. Chem. Chem. Phys.*, 2017, **19**, 2940–2949.
- J. Ma and X. Zhang, *J. Mater. Chem.*, 2016, **4**, 10008–10013.
- B. Sun, K. Kretschmer, X. Xie, P. Munroe, Z. Peng and G. Wang, *Adv. Mater.*, 2017, 1606816.
- C. Xia, R. Black, R. Fernandes, B. Adams and L. F. Nazar, *Nat. Chem.*, 2015, **7**, 496–501.

- 43 C. Xia, R. Fernandes, F. H. Cho, N. Sudhakar, B. Buonacorsi, S. Walker, M. Xu, J. Baugh and L. F. Nazar, *J. Am. Chem. Soc.*, 2016, **138**, 11219–11226.
- 44 L. Lutz, W. Yin, A. Grimaud, D. A. D. Corte, M. Tang, L. Johnson, E. Azaceta, V. Sarou-Kanian, A. J. Naylor, S. Hamad, J. A. Anta, E. Salager, R. Tena-Zaera, P. G. Bruce and J.-M. Tarascon, *J. Phys. Chem. C*, 2016, **120**, 20068–20076.
- 45 X. Bi, R. Wang, L. Ma, D. Zhang, K. Amine and J. Lu, *Small Methods*, 2017, **1**, 1700102.
- 46 H. Yadegari, M. Norouzi Banis, A. Lushington, Q. Sun, R. Li, T.-K. Sham and X. Sun, *Energy Environ. Sci.*, 2017, **10**, 286–295.
- 47 Q. Sun, J. Liu, X. Li, B. Wang, H. Yadegari, A. Lushington, M. N. Banis, Y. Zhao, W. Xiao, N. Chen, J. Wang, T.-K. Sham and X. Sun, *Adv. Funct. Mater.*, 2017, **27**, 1606662.
- 48 F. Wu, Y. Xing, J. Lai, X. Zhang, Y. Ye, J. Qian, L. Li and R. Chen, *Adv. Funct. Mater.*, 2017, **27**, 1700632.
- 49 J.-H. Kang, W.-J. Kwak, D. Aurbach and Y.-K. Sun, *J. Mater. Chem. A*, 2017, **5**, 20678–20686.
- 50 S. Ma, W. C. McKee, J. Wang, L. Guo, M. Jansen, Y. Xu and Z. Peng, *Phys. Chem. Chem. Phys.*, 2017, **19**, 12375–12383.
- 51 Z.-L. Wang, D. Xu, J.-J. Xu and X.-B. Zhang, *Chem. Soc. Rev.*, 2014, **43**, 7746–7786.
- 52 G. M. Veith, J. Nanda, L. H. Delmau and N. J. Dudney, *J. Phys. Chem. Lett.*, 2012, **3**, 1242–1247.
- 53 G. M. Veith, N. J. Dudney, J. Howe and J. Nanda, *J. Phys. Chem. C*, 2011, **115**, 14325–14333.
- 54 P. Du, J. Lu, K. C. Lau, X. Luo, J. Bareno, X. Zhang, Y. Ren, Z. Zhang, L. A. Curtiss, Y.-K. Sun and K. Amine, *Phys. Chem. Chem. Phys.*, 2013, **15**, 5572–5581.
- 55 N. Feng, P. He and H. Zhou, *Adv. Energy Mater.*, 2016, **6**, 1502303.
- 56 R. Black, S. H. Oh, J.-H. Lee, T. Yim, B. Adams and L. F. Nazar, *J. Am. Chem. Soc.*, 2012, **134**, 2902–2905.
- 57 E. Nasybulin, W. Xu, M. H. Engelhard, Z. Nie, X. S. Li and J.-G. Zhang, *J. Power Sources*, 2013, **243**, 899–907.
- 58 C. V. Amanchukwu, J. R. Harding, Y. Shao-Horn and P. T. Hammond, *Chem. Mater.*, 2014, **27**, 550–561.
- 59 J. R. Harding, C. V. Amanchukwu, P. T. Hammond and Y. Shao-Horn, *J. Phys. Chem. C*, 2015, **119**, 6947–6955.
- 60 Z. E. M. Reeve, C. J. Franko, K. J. Harris, H. Yadegari, X. Sun and G. R. Goward, *J. Am. Chem. Soc.*, 2016, **139**, 595–598.
- 61 Q. Sun, H. Yadegari, M. N. Banis, J. Liu, B. Xiao, X. Li, C. Langford, R. Li and X. Sun, *J. Phys. Chem. C*, 2015, **119**, 13433–13441.
- 62 Z. Jian, Y. Chen, F. Li, T. Zhang, C. Liu and H. Zhou, *J. Power Sources*, 2014, **251**, 466–469.
- 63 N. Zhao, C. Li and X. Guo, *Phys. Chem. Chem. Phys.*, 2014, **16**, 15646–15652.
- 64 C. L. Bender, W. Bartuli, M. G. Schwab, P. Adelhelm and J. Janek, *Energy Technol.*, 2015, **3**, 242–248.
- 65 W.-W. Yin, Z. Shadike, Y. Yang, F. Ding, L. Sang, H. Li and Z.-W. Fu, *Chem. Commun.*, 2015, **51**, 2324–2327.
- 66 G. A. Elia, I. Hasa and J. Hassoun, *Electrochim. Acta*, 2016, **191**, 516–520.
- 67 S. J. Higgins, *Chem. Soc. Rev.*, 1997, **26**, 247–257.
- 68 O. Ingnas, *Chem. Soc. Rev.*, 2010, **39**, 2633–2642.
- 69 X. Guo, A. Facchetti and T. J. Marks, *Chem. Rev.*, 2014, **114**, 8943–9021.
- 70 M. B. Smith and J. March, *March's Advanced Organic Chemistry*, John Wiley & Sons, Inc., 6th edn, 2006, pp. 296–327.
- 71 D. T. Sawyer and J. S. Valentine, *Acc. Chem. Res.*, 1981, **14**, 393–400.
- 72 M. Hayyan, M. A. Hashim and I. M. AlNashef, *Chem. Rev.*, 2016, **116**, 3029–3085.
- 73 F. Mizuno, S. Nakanishi, Y. Kotani, S. Yokoishi and H. Iba, *Electrochemistry*, 2010, **78**, 403–405.
- 74 S. A. Freunberger, Y. Chen, Z. Peng, J. M. Griffin, L. J. Hardwick, F. Barde, P. Novak and P. G. Bruce, *J. Am. Chem. Soc.*, 2011, **133**, 8040–8047.
- 75 J. Xiao, J. Hu, D. Wang, D. Hu, W. Xu, G. L. Graff, Z. Nie, J. Liu and J.-G. Zhang, *J. Power Sources*, 2011, **196**, 5674–5678.
- 76 S. A. Freunberger, Y. Chen, N. E. Drewett, L. J. Hardwick, F. Bardé and P. G. Bruce, *Angew. Chem.*, 2011, **50**, 8609–8613.
- 77 M. Marinaro, S. Theil, L. Jörissen and M. Wohlfahrt-Mehrens, *Electrochim. Acta*, 2013, **108**, 795–800.
- 78 W. Xu, J. Hu, M. H. Engelhard, S. A. Towne, J. S. Hardy, J. Xiao, J. Feng, M. Y. Hu, J. Zhang, F. Ding, M. E. Gross and J.-G. Zhang, *J. Power Sources*, 2012, **215**, 240–247.
- 79 K. U. Schwenke, S. Meini, X. Wu, H. A. Gasteiger and M. Piana, *Phys. Chem. Chem. Phys.*, 2013, **15**, 11830–11839.
- 80 C. O. Laoire, S. Mukerjee, E. J. Plichta, M. a. Hendrickson and K. M. Abraham, *J. Electrochem. Soc.*, 2011, **158**, 302.
- 81 H.-G. Jung, J. Hassoun, J.-B. Park, Y.-K. Sun and B. Scrosati, *Nat. Chem.*, 2012, **4**, 579–585.
- 82 N. Zhao and X. Guo, *J. Phys. Chem. C*, 2015, **119**, 25319–25326.
- 83 S. Meini, M. Piana, N. Tsiouvaras, A. Garsuch and H. A. Gasteiger, *Electrochem. Solid-State Lett.*, 2012, **15**, A45–A48.
- 84 Z. Guo, X. Dong, S. Yuan, Y. Wang and Y. Xia, *J. Power Sources*, 2014, **264**, 1–7.
- 85 M. H. Cho, J. Trottier, C. Gagnon, P. Hovington, D. Clément, A. Vijh, C.-S. Kim, A. Guerfi, R. Black, L. Nazar and K. Zaghib, *J. Power Sources*, 2014, **268**, 565–574.
- 86 K. U. Schwenke, M. Metzger, T. Restle, M. Piana and H. A. Gasteiger, *J. Electrochem. Soc.*, 2015, **162**, A573–A584.
- 87 N. B. Aetukuri, B. D. McCloskey, J. M. García, L. E. Krupp, V. Viswanathan and A. C. Luntz, *Nat. Chem.*, 2015, **7**, 50–56.
- 88 R. Pinedo, D. A. Weber, B. Bergner, D. Schröder, P. Adelhelm and J. Janek, *J. Phys. Chem. C*, 2016, **120**, 8472–8481.
- 89 J. Kim, H. Park, B. Lee, W. M. Seong, H.-D. Lim, Y. Bae, H. Kim, W. K. Kim, K. H. Ryu and K. Kang, *Nat. Commun.*, 2016, **7**, 10670.
- 90 H. Yadegari, M. N. Banis, B. Xiao, Q. Sun, X. Li, A. Lushington, B. Wang, R. Li, T.-K. Sham, X. Cui and X. Sun, *Chem. Mater.*, 2015, **27**, 3040–3047.
- 91 D. Sharon, M. Afri, M. Noked, A. Garsuch, A. A. Frimer and D. Aurbach, *J. Phys. Chem. Lett.*, 2013, **4**, 3115–3119.
- 92 D. Sharon, V. Etacheri, A. Garsuch, M. Afri, A. A. Frimer and D. Aurbach, *J. Phys. Chem. Lett.*, 2012, **4**, 127.
- 93 V. S. Bryantsev and F. Faglioni, *J. Phys. Chem.*, 2012, **116**, 7128–7138.
- 94 Z. Xue, D. He and X. Xie, *J. Mater. Chem.*, 2015, **3**, 19218–19253.